Geophysical Monograph Series

175 **A Continental Plate Boundary: Tectonics at South Island, New Zealand** *David Okaya, Tim Stem, and Fred Davey (Eds.)*
176 **Exploring Venus as a Terrestrial Planet** *Larry W. Esposito, Ellen R. Stofan, and Thomas E. Cravens (Eds.)*
177 **Ocean Modeling in an Eddying Regime** *Matthew Hecht and Hiroyasu Hasumi (Eds.)*
178 **Magma to Microbe: Modeling Hydrothermal Processes at Oceanic Spreading Centers** *Robert P. Lowell, Jeffrey S. Seewald, Anna Metaxas, and Michael R. Perfit (Eds.)*
179 **Active Tectonics and Seismic Potential of Alaska** *Jeffrey T. Freymueller, Peter J. Haeussler, Robert L. Wesson, and Göran Ekström (Eds.)*
180 **Arctic Sea Ice Decline: Observations, Projections, Mechanisms, and Implications** *Eric T. DeWeaver, Cecilia M. Bitz, and L.-Bruno Tremblay (Eds.)*
181 **Midlatitude Ionospheric Dynamics and Disturbances** *Paul M. Kintner, Jr., Anthea J. Coster, Tim Fuller-Rowell, Anthony J. Mannucci, Michael Mendillo, and Roderick Heelis (Eds.)*
182 **The Stromboli Volcano: An Integrated Study of the 2002–2003 Eruption** *Sonia Calvari, Salvatore Inguaggiato, Giuseppe Puglisi, Maurizio Ripepe, and Mauro Rosi (Eds.)*
183 **Carbon Sequestration and Its Role in the Global Carbon Cycle** *Brian J. McPherson and Eric T. Sundquist (Eds.)*
184 **Carbon Cycling in Northern Peatlands** *Andrew J. Baird, Lisa R. Belyea, Xavier Comas, A. S. Reeve, and Lee D. Slater (Eds.)*
185 **Indian Ocean Biogeochemical Processes and Ecological Variability** *Jerry D. Wiggert, Raleigh R. Hood, S. Wajih A. Naqvi, Kenneth H. Brink, and Sharon L. Smith (Eds.)*
186 **Amazonia and Global Change** *Michael Keller, Mercedes Bustamante, John Gash, and Pedro Silva Dias (Eds.)*
187 **Surface Ocean–Lower Atmosphere Processes** *Corinne Le Quèrè and Eric S. Saltzman (Eds.)*
188 **Diversity of Hydrothermal Systems on Slow Spreading Ocean Ridges** *Peter A. Rona, Colin W. Devey, Jérôme Dyment, and Bramley J. Murton (Eds.)*
189 **Climate Dynamics: Why Does Climate Vary?** *De-Zheng Sun and Frank Bryan (Eds.)*
190 **The Stratosphere: Dynamics, Transport, and Chemistry** *L. M. Polvani, A. H. Sobel, and D. W. Waugh (Eds.)*
191 **Rainfall: State of the Science** *Firat Y. Testik and Mekonnen Gebremichael (Eds.)*
192 **Antarctic Subglacial Aquatic Environments** *Martin J. Siegert, Mahlon C. Kennicut II, and Robert A. Bindschadler*
193 **Abrupt Climate Change: Mechanisms, Patterns, and Impacts** *Harunur Rashid, Leonid Polyak, and Ellen Mosley-Thompson (Eds.)*
194 **Stream Restoration in Dynamic Fluvial Systems: Scientific Approaches, Analyses, and Tools** *Andrew Simon, Sean J. Bennett, and Janine M. Castro (Eds.)*
195 **Monitoring and Modeling the *Deepwater Horizon* Oil Spill: A Record-Breaking Enterprise** *Yonggang Liu, Amy MacFadyen, Zhen-Gang Ji, and Robert H. Weisberg (Eds.)*
196 **Extreme Events and Natural Hazards: The Complexity Perspective** *A. Surjalal Sharma, Armin Bunde, Vijay P. Dimri, and Daniel N. Baker (Eds.)*
197 **Auroral Phenomenology and Magnetospheric Processes: Earth and Other Planets** *Andreas Keiling, Eric Donovan, Fran Bagenal, and Tomas Karlsson (Eds.)*
198 **Climates, Landscapes, and Civilizations** *Liviu Giosan, Dorian Q. Fuller, Kathleen Nicoll, Rowan K. Flad, and Peter D. Clift (Eds.)*
199 **Dynamics of the Earth's Radiation Belts and Inner Magnetosphere** *Danny Summers, Ian R. Mann, Daniel N. Baker, and Michael Schulz (Eds.)*
200 **Lagrangian Modeling of the Atmosphere** *John Lin (Ed.)*
201 **Modeling the Ionosphere-Thermosphere** *Jospeh D. Huba, Robert W. Schunk, and George V. Khazanov (Eds.)*
202 **The Mediterranean Sea: Temporal Variability and Spatial Patterns** *Gian Luca Eusebi Borzelli, Miroslav Gacic, Piero Lionello, and Paola Malanotte-Rizzoli (Eds.)*
203 **Future Earth - Advancing Civic Understanding of the Anthropocene** *Diana Dalbotten, Gillian Roehrig, and Patrick Hamilton (Eds.)*
204 **The Galápagos: A Natural Laboratory for the Earth Sciences** *Karen S. Harpp, Eric Mittelstaedt, Noémi d'Ozouville, and David W. Graham (Eds.)*
205 **Modeling Atmospheric and Oceanic Flows: Insights from Laboratory Experiments and Numerical Simulations** *Thomas von Larcher and Paul D. Williams (Eds.)*
206 **Remote Sensing of the Terrestrial Water Cycle** *Venkat Lakshmi (Eds.)*
207 **Magnetotails in the Solar System** *Andreas Keiling, Caitríona Jackman, and Peter Delamere (Eds.)*
208 **Hawaiian Volcanoes: From Source to Surface** *Rebecca Carey, Valerie Cayol, Michael Poland, and Dominique Weis (Eds.)*
209 **Sea Ice: Physics, Mechanics, and Remote Sensing** *Mohammed Shokr and Nirmal Sinha (Eds.)*
210 **Fluid Dynamics in Complex Fractured-Porous Systems** *Boris Faybishenko, Sally M. Benson, and John E. Gale (Eds.)*
211 **Subduction Dynamics: From Mantle Flow to Mega Disasters** *Gabriele Morra, David A. Yuen, Scott King, Sang Mook Lee, and Seth Stein (Eds.)*
212 **The Early Earth: Accretion and Differentiation** *James Badro and Michael Walter(Eds.)*
213 **Global Vegetation Dynamics: Concepts and Applications in the MC1 Model** *Dominique Bachelet and David Turner (Eds.)*
214 **Extreme Events: Observations, Modeling and Economics** *Mario Chavez, Michael Ghil, and Jaime Urrutia-Fucugauchi (Eds.)*
215 **Auroral Dynamics and Space Weather** *Yongliang Zhang and Larry Paxton (Eds.)*

Geophysical Monograph 216

Low-Frequency Waves in Space Plasmas

Andreas Keiling
Dong-Hun Lee
Valery Nakariakov
Editors

This Work is a co-publication between the American Geophysical Union and John Wiley and Sons, Inc.

AGU
American Geophysical Union

WILEY

This Work is a co-publication between the American Geophysical Union and John Wiley & Sons, Inc.

Published under the aegis of the AGU Publications Committee

Brooks Hanson, Director of Publications
Robert van der Hilst, Chair, Publications Committee

Published by John Wiley & Sons, Inc., Hoboken, New Jersey
Published simultaneously in Canada

Library of Congress Cataloging-in-Publication Data is available.

ISBN: 978-1-119-05495-5

Cover image: Global hybrid simulation of foreshock ULF waves (Nick Omidi, Chapter 13). (inset, top) Transverse oscillations of coronal loops (Tongjiang Wang, Chapter 23). (inset, bottom) All-sky image of auroral beads (I. Jonathan Rae, Chapter 7).

Printed in the United States of America

10 9 8 7 6 5 4 3 2 1

CONTENTS

CONTRIBUTORS

Vassilis Angelopoulos
Department of Earth
Planetary and Space Sciences
UCLA, Los Angeles, California, USA

D. Banerjee
Indian Institute of Astrophysics
Koramangala, Bengaluru, India

Scott A. Boardsen
Goddard Planetary Heliophysics
Institute University of Maryland
Baltimore, Maryland, USA

Heliophysics Science Division
NASA Goddard Space Flight Center
Greenbelt, Maryland, USA

Jacob Bortnik
Department of Atmospheric and Oceanic Sciences
UCLA, Los Angeles, California, USA

Paul S. Cally
School of Mathematical Sciences, Monash
University, Clayton, Victoria, Australia

Lunjin Chen
Department of Physics, University of Texas at
Dallas, Richardson, Texas, USA

P. F. Chen
School of Astronomy and Space Science
Nanjing University
Nanjing, China

Fabien Darrouzet
Belgian Institute for Space Aeronomy
Brussels, Belgium

P. A. Delamere
Geophysical Institute
University of Alaska Fairbanks
Fairbanks, Alaska, USA

E. Dubinin
Max-Planck-Institute for Solar System Research
Göttingen, Germany

Bengt Eliasson
Department of Astronomy
University of Maryland
College Park, Maryland, USA

SUPA, Physics Department
University of Strathclyde
Glasgow, Scotland, UK

M. Fraenz
Max-Planck-Institute for Solar System Research
Göttingen, Germany

M. Fujimoto
Institute of Space and Astronautical Science
Japan Aerospace Exploration Agency
Sagamihara, Kanagawa, Japan

Y. Harada
Space Sciences Laboratory
University of California
Berkeley, California, USA

J. S. Halekas
Department of Physics and Astronomy
University of Iowa
Iowa City, Iowa, USA

Balazs Heilig
Geological and Geophysical Institute of Hungary
Tihany, Hungary

Kyoung-Joo Hwang
NASA Goddard Space Flight Center
Greenbelt, Maryland, USA

University of Maryland
Baltimore, Maryland, USA

M. K. James
Department of Physics and Astronomy
University of Leicester
Leicester, UK

David B. Jess
Astrophysics Research Centre
School of Mathematics and Physics
Queen's University Belfast
Belfast, Northern Ireland, UK

L.K. Jian
Department of Astronomy, University of Maryland
College Park, Maryland, USA

Jay R. Johnson
Princeton Center for Heliophysics and Princeton
Plasma Physics Laboratory
Princeton University
Princeton, New Jersey, USA

Eun-Hwa Kim
Princeton Center for Heliophysics and Princeton
Plasma Physics Laboratory
Princeton University,
Princeton, New Jersey, USA

Craig A. Kletzing
Department of Physics and Astronomy
University of Iowa
Iowa City, Iowa, USA

Dmitri Yu. Klimushkin
Institute of Solar-Terrestrial Physics SB RAS
Irkutsk, Russia

H. Kojima
Research Institute for Sustainable
Humanosphere
Kyoto University
Uji, Kyoto, Japan

D. A. Kozlov
Institute of Solar-Terrestrial Physics SB RAS
Irkutsk, Russia

A. S. Leonovich
Institute of Solar-Terrestrial Physics SB RAS
Irkutsk, Russia

Wen Li
Department of Atmospheric and
Oceanic Sciences
UCLA, Los Angeles, California, USA

Pavel N. Mager
Institute of Solar-Terrestrial Physics SB RAS
Irkutsk, Russia

Ian R. Mann
Department of Physics
University of Alberta
Edmonton, Alberta, Canada

V. A. Mazur
Institute of Solar-Terrestrial Physics SB RAS
Irkutsk, Russia

Gennady M. Milikh
Department of Astronomy
University of Maryland
College Park, Maryland, USA

Hamed Moradi
Trinity College
The University of Melbourne
Parkville, Australia

Fabrice Mottez
Laboratoire Univers et Théories
Observatoire de Paris
CNRS, Université Paris Diderot
Meudon, France

T. Nagai
Department of Earth and Planetary Sciences,
Tokyo Institute of Technology
Meguro-ku, Tokyo, Japan

Amir Najmi
Department of Astronomy
University of Maryland
College Park, Maryland, USA

Tomoko Nakagawa
Information and Communication Engineering
Tohoku Institute of Technology
Sendai, Miyagi, Japan

Yukitoshi Nishimura
Department of Atmospheric and Oceanic Sciences
UCLA, Los Angeles, California, USA

L. Ofman
Catholic University of America and Code 671
NASA Goddard Space Flight Center
Greenbelt, Maryland, USA

N. Omidi
Solana Scientific Inc.
Solana Beach, California, USA

K. Dennis Papadopoulos
Department of Astronomy
University of Maryland
College Park, Maryland, USA

Viacheslav A. Pilipenko
Space Research Institute
Moscow, Russia

F. Plaschke
Space Research Institute
Austrian Academy of Sciences
Graz, Austria

S. Krishna Prasad
Astrophysics Research Centre
School of Mathematics and Physics
Queens University Belfast
Belfast, Northern Ireland, UK

I. Jonathan Rae
Department of Space and Climate Physics
Mullard Space Science Laboratory
Holmbury St. Mary, Dorking, Surrey, UK

S. P. Rajaguru
Indian Institute of Astrophysics
Bangalore, India

C. T. Russell
Department of Earth
Planetary and Space Sciences
University of California
Los Angeles, California, USA

Xi Shao
Department of Astronomy
University of Maryland
College Park, Maryland, USA

A. Surjalal Sharma
Department of Astronomy
University of Maryland
College Park, Maryland, USA

David G. Sibeck
NASA Goddard Space Flight Center
Greenbelt, Maryland, USA

Robert Sych
Institute of Solar-Terrestrial Physics SB RAS
Irkutsk, Russia

I. Shinohara
Institute of Space and Astronautical Science,
Japan Aerospace Exploration Agency,
Sagamihara, Kanagawa, Japan

James A. Slavin
Department of Atmospheric, Oceanic and
Space Sciences
University of Michigan
Ann Arbor, Michigan, USA

Kazue Takahashi
The Johns Hopkins University Applied Physics
Laboratory
Laurel, Maryland, USA

Richard M. Thorne
Department of Atmospheric and
Oceanic Sciences,
UCLA, Los Angeles, California, USA

Maria E. Usanova
Laboratory for Atmospheric and
Space Physics
University of Colorado at Boulder
Boulder, Colorado, USA

Aram Vartanyan
Department of Astronomy
University of Maryland
College Park
Maryland, USA

Gary Verth
Solar Physics and Space Plasma Research
Centre (SP^2RC)
The University of Sheffield
Sheffield, UK

Martin Volwerk
Space Research Institute
Austrian Academy of Sciences
Graz, Austria

T. J. Wang
Department of Physics
The Catholic University of America
Washington, DC

NASA Goddard Space Flight Center,
Code 671
Greenbelt, Maryland, USA

Clare E. J. Watt
Department of Meteorology
University of Reading, Earley Gate
Reading, UK

H.Y. Wei
Department of Earth
Planetary and Space Sciences
University of California
Los Angeles, California, USA

Lynn B. Wilson, III
NASA Goddard Space Flight Center
Heliophysics Science Division
USA

Tim K. Yeoman
Department of Physics and Astronomy
University of Leicester
Leicester, UK

S. Zenitani
National Astronomical Observatory of Japan
Mitaka, Tokyo, Japan

PREFACE

Low-frequency waves in space plasmas have been studied for many decades, and our knowledge gain has been incremental with several paradigm-changing leaps forward. In our solar system, such waves occur in the ionospheres and magnetospheres of planets (Earth, Mercury, Jupiter, Saturn, etc.) and around our Moon. They occur in the solar wind, and more recently, they have been confirmed in the Sun's atmosphere as well. For the purpose of this book, we define the range of low-frequency waves to lie between 1 mHz and 30 kHz, thus including ULF, ELF, and VLF waves.

Recently, there has been an abundance of new wave observations from spacecraft missions, such as MESSENGER, Geotail, Cluster, THEMIS, ARTEMIS, Van Allen Probes, Galileo, STEREO, CHAMPS, New Horizons, Cassini, TRACE, Hinode, SDO—to name a few. On the ground, magnetometer arrays and radar networks have expanded to detect low-frequency signals on a global scale with high timing accuracy. In addition, there have been tremendous advances in the capabilities of simulations to allow modeling many of the relevant processes.

This monograph reviews recent advances of wave research in various space plasmas of our solar system, addressing various aspects of wave physics. The main objective is to give a concise and authoritative up-to-date look on where wave research stands: What do we know? What have we learned in the last decade? What are unanswered questions?

The book is organized into ten sections, each representing a specific region in the solar system. The thread of the ten sections begins with waves at Earth's ionosphere and progresses outward to various regions of Earth's magnetosphere. Then, beyond geospace, waves in the solar wind, at the Moon, and at other planets' magnetospheres are reviewed. The book finishes with waves in the Sun's atmosphere. Below we list the many reviewers who helped in assuring that each chapter is of highest quality.

While in the past waves in different astrophysical plasmas have been largely treated in separate books, the unique feature of this monograph is that it covers waves occurring in many plasma regions of our solar system. As a result this book should appeal to a broad community of space scientists, and it should also be of interest to astronomers/astrophysicists who are studying space plasmas beyond our solar system.

Last, we note that many of the chapters are born out of presentations given at the Chapman conference on "Low-Frequency Waves in Space Plasmas," held on Jeju Island, Republic of Korea, during the first week of September 2014, with an attendance of about 120 scientists. At the conference, the breadth of topics covered stimulated cross-disciplinary discussions among scientists specializing in all aspects of wave physics.

Andreas Keiling
University of California at Berkeley, USA

Dong-Hun Lee
Kyung Hee University, Republic of Korea

Valery Nakariakov
University of Warwick, UK

Reviewers (in alphabetical order):

Andrey Afanasyev, Mats André, Sergey Anfinogentov, Inigo Arregui, Dipankar Banerjee, Xochitl Blanco-Cano, Doug Braun, David Burgess, Cristina Cadavid, Manuel Collados, Frank Crary, Mark Engebretson, Jared Espley, Shigeru Fujita, Michael Hartinger, Balazs Heilig, Bogdan Hnat, George Hospodarsky, Kyoung-Joo Hwang, Philip Isenberg, Peter Israelevich, Jay Johnson, Yoshiya Kasahara, Hyomin Kim, Dimitri Klimushkin, Guan Le, Jun Liang, Wei Liu, Wenlong Liu, Robert Lysak, Shinobu Machida, Evgeny Mishin, Giuseppe Nistico, Leon Ofman, Nick Omidi, Slava Pilipenko, Douglas Rabin, Jim Raines, Robert Rankin, Craig Rodger, Yoshifumi Saito, Abhishek Shrivastava, Mikhail Sitnov, Gabriella Sternberg, Danny Summers, Takeru Suzuki, Kazue Takahashi, Teiji Uozumi, Tom Van Doorsselaere, Gary Verth, Colin Waters, Clare Watt, Hanying Wei, Peter Yoon, Tielong Zhang, Qiugang Zong.

Section I
Ionosphere

1

Energetic Particle-Driven ULF Waves in the Ionosphere

T. K. Yeoman,[1] M. K. James,[1] D. Yu. Klimushkin,[2] and P. N. Mager[2]

1.1. INTRODUCTION

Ionospheric radar systems have proved to be a powerful tool for the investigation of magnetospheric ULF waves. Because of their multipoint remote sensing capability, they are suitable for tracking waves with periods in the Pc3–5 bands (frequencies of 100–2 mHz). The high spatial resolutions (typically 15–45 km) they produce of the wave ionospheric electric field have provided direct information as to the ionospheric boundary conditions determined by the ionospheric Pedersen conductivity, rather than being sensitive to the ionospheric Hall currents which provide the magnetic field signature most commonly measured by ground magnetometer systems. Magnetospheric ULF waves are generally classified into one of two types, depending on whether their polarization is predominantly toroidal or poloidal. Toroidal waves are those in which the magnetic field oscillates in the azimuthal direction and are characterized by low effective azimuthal wave numbers (m), or equivalently by large azimuthal scale sizes. Conversely, poloidal waves oscillate with a magnetic field in the meridional direction with high m numbers (a smaller azimuthal scale size). Both toroidal and poloidal ULFwaves propagate as Alfvén standing waves between the two conjugate endpoints of the magnetic field at the Earth's ionosphere. Low-m (toroidal) waves are generally thought to have their energy source external to the magnetosphere. High-m (poloidal) events usually have a different generation mechanism to the low-m events, where the energy source is thought to be from energetic particle populations within the magnetosphere, which may be transferred from the particles into the wave within the collisionless magnetosphere via wave–particle interactions. The energetic particle populations generating high-m waves enter the inner dipolar magnetosphere from the magnetotail, whereupon they gradient-curvature drift around the planet, forming part of the global ring current.

Both toroidal and poloidal ULF waves are changed as they pass from the magnetosphere through the ionosphere, where they undergo rotation and attenuation. It is assumed that on passage through the conducting, vertically stratified ionosphere above the insulating atmosphere, the Alfvén wave will rotate 90°. Thereupon the azimuthal magnetic field component in the magnetosphere is detected on the ground as a north–south magnetic field perturbation [*Hughes and Southwood*, 1976]. The attenuation that occurs is proportional to $e^{-|k|z}$, where |k| is the field-perpendicular value of the wavenumber and z is the E-region height. The greater the attenuation is, the smaller is the field-perpendicular scale size of the wave.

Consequently high-m poloidal waves become much more attenuated in ground magnetometer data than low-m toroidal waves. For this reason ionospheric radar systems have been effective in the study of high-m poloidal waves driven by energetic particle populations within

[1]*Department of Physics and Astronomy, University of Leicester, Leicester, UK*

[2]*Institute of Solar-Terrestrial Physics SB RAS, Irkutsk, Russia*

Low-Frequency Waves in Space Plasmas, Geophysical Monograph 216, First Edition.
Edited by Andreas Keiling, Dong-Hun Lee, and Valery Nakariakov.

the magnetosphere, and it is this class of ULF waves that will be discussed in this chapter. These ULF waves are implicated in the energization (e.g., *O'Brien et al*. [2003]) and decay (e.g., *Baddeley et al*. [2004]) of radiation belt particles, which is an area of considerable current research interest. The frequency, polarization, and azimuthal structure of the waves are key elements in controlling this energy exchange [*Elkington*, 2006], and hence ionospheric observations of high-*m* ULF waves have an important role to play in furthering our understanding of the wave characteristics, and their role in radiation belt physics.

In order for a high-*m*, poloidal wave to be generated, two conditions must be satisfied. First, there must be a source of free energy for wave growth within the particle population, and second, the spatial and temporal evolution of the waves and the particles must match via a resonance condition, such that the free energy has an opportunity to transfer from the particles to the waves. The usual free energy condition is one that requires that the particle distribution function, f, increases with particle energy, W,

$$\frac{\mathrm{d}f}{\mathrm{d}W} = \frac{\partial f}{\partial W} + \frac{\mathrm{d}L}{\mathrm{d}W}\frac{\partial f}{\partial L} > 0, \tag{1.1}$$

(e.g., *Southwood and Hughes* [1983], *Mann and Chisham* [2000]), where L is the L-shell under consideration. Thus instability can occur if there is a sufficiently large spatial gradient ($\partial f / \partial L$) in the distribution, or if a population inversion occurs at some point in the distribution ($\partial f / \partial W > 0$), usually referred to as a non-Maxwellian or bump-on-tail distribution [*Southwood et al*., 1969].

The resonance condition, which is also required to be met for effective energy transfer from the particles to the wave, is given by

$$\omega_{wave} - m_{wave}\omega_d = N\omega_b, \tag{1.2}$$

where ω_{wave}, ω_b, and ω_d are the angular frequencies of the wave, the proton bounce, and the proton azimuthal drift, respectively [*Southwood et al*., 1969]. In drift-bounce resonance N is an integer (usually ±1). Where the particle bounce is not required for the resonance condition, Equation (1.2) reduces to the $N = 0$, drift resonance case,

$$\omega_{wave} = m_{wave}\omega_d \tag{1.3}$$

An early confirmation of these ideas came from *Hughes et al*. [1978], who were able to use the ATS6 geostationary spacecraft to measure both the wave field and a population inversion in the driving particle population for a wave attributed to the drift-bounce mechanism. More recently, convincing evidence of a drift-bounce resonance wave and its driving particle population were presented by *Liu et al*. [2013], based on THEMIS particle and field data. However, to this day such datasets have proved to be rare and elusive, and a variety of techniques have had to be harnessed to progress our understanding of wave–particle interactions in the magnetosphere.

While many of the characteristics of high-*m* ULF waves can be explained by the drift resonance conditions defined in Equations (1.2) and (1.3), these equations do not offer an explanation of the latitudinal phase structure. The latitudinal phase structure is likely determined by the particle distributions driving the waves, and ionospheric observations have revealed a wide variety of such structures.

Mager and Klimushkin [2008] and *Mager et al*. [2009] have suggested the possible role of the radial structure of a cloud of injected energetic particles driving a high-*m* wave in determining the latitudinal phase structure of the wave. *Mager et al*. [2009] considered waves of form $e^{im\varphi}$ where φ is the azimuthal angle. Assuming the local field line eigenfrequency is $\omega(x)$ where x is the radial coordinate, and that the wave source is a local inhomogeneity resulting from particle injection drifting at speed $\omega_d(x)$, producing a nonsteady current $j(t)$, *Mager et al*. [2009] showed that the wave phase is then given by

$$\Psi = -\omega(x)t + \frac{\omega(x)}{\omega_d(x)}\varphi \tag{1.4}$$

An example of the phase evolution determined by *Mager et al*. [2009] is illustrated in the $x-\varphi$ plane in Figure 1.1. If the particle drift velocity grows with the radial coordinate, x, then the particle cloud is stretched into a spiral in the equatorial plane. Near the source the phase follows the source closely. The variation of the particle drift with x may then result in an inwards phase motion (a negative wavevector k_x), which will manifest itself as an equatorward phase motion in the ionosphere. This equatorward phase motion would reverse to poleward (a positive wavevector k_x) at a later time further from the source as the natural frequency of the field lines becomes important. This transition is marked in Figure 1.1 by the line $k_x = 0$. A particle drift velocity decreasing with radial coordinate would show poleward phase propagation throughout. Such features in the latitudinal phase structure of high-*m* waves have been observed and are discussed in later sections. The wave features predicted by such a moving source are not in conflict with the drift and drift-bounce mechanisms outlined above, as any wave event generated by a moving particle cloud source may be enhanced and sustained by these energy sources.

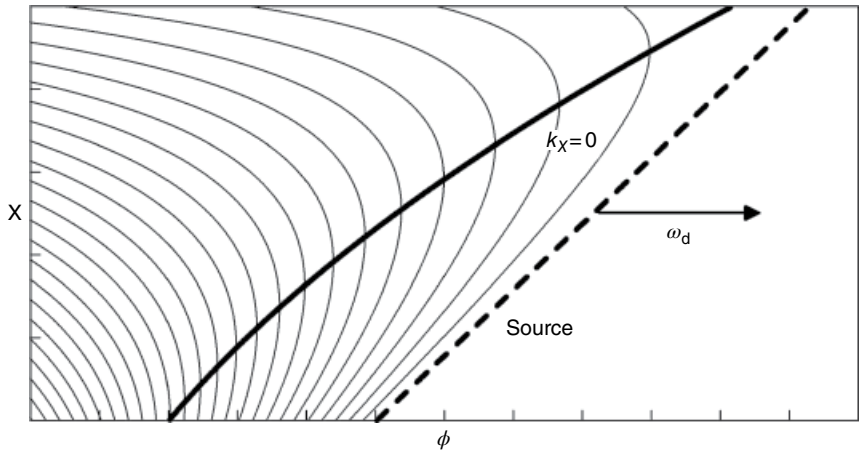

Figure 1.1 Lines of constant phase for a wave driven by a localized cloud of westward-drifting protons whose drift velocity increases with the radial coordinate *x*. From *Mager et al.* [2009].

1.2. EARLY RADAR OBSERVATIONS

The first opportunities for ionospheric observations of high-*m* ULF waves in the ionosphere came with the development of coherent scatter radars. Early oscillations associated with ULF waves were reported in the 1960s (e.g., *Keys* [1965]), but the development of very high frequency (VHF) coherent scatter radars such as the Scandinavian Twin Auroral Radar Experiment (STARE; *Greenwald et al.* [1978]) and the Sweden and Britain Radar experiment (SABRE; *Nielsen et al.* [1983]) provided major new datasets that transformed our knowledge of these phenomena. Early results from the STARE system [*Walker et al.*, 1979] focused on low-*m* waves where ground-based magnetometer data were also available, and provided important confirmation of the field line resonance theory of *Southwood* [1974] and *Chen and Hasegawa* [1974], showing a clear ampliude maximum coincident with a 180° poleward phase change in latitude. However observations of high-*m* ULF waves followed shortly after, and a new class of ULF waves, termed "storm-time" Pc5 waves were discovered [*Allan et al.*, 1982, 1983a, b; *Walker et al.*, 1982]. These waves were identified as compressional waves of high *m* number ($m = -20$ to -80) with periods in the Pc5 range (200–400 s), predominantly observed in the dusk sector of the ionosphere during disturbed magnetic conditions. The ionospheric wave electric fields were small and linearly polarized, with similar magnitudes in the north–south and east–west components. In contrast to the low-*m* wave observations of *Walker et al.* [1979], little phase variation in latitude was observed. The waves were attributed to the drift-resonance source mechanism described by Equation (1.3), with the responsible particle population being westward-drifting protons of energy 20–80 keV, and were the first radar observations of waves not attributed to a driving mechanism external to the Earth's magnetosphere.

At a similar time another population of waves with unusual latitudinal phase variation were observed by the SABRE radar [*Waldock et al.*, 1983], an example of which is reproduced here in Figure 1.2. In this case an equatorward phase propagation was seen, and again the wave events were associated with the dusk sector. Subsequent analysis of the occurrence statistics of these waves by *Tian et al.* [1991] led to the conclusion that they were associated with the plasmapause, as they occurred at a local time when the plasmapause lay within the radar field of view. However, similar observations from the higher latitude Bistatic Auroral Radar System (BARS; *McNamara et al.* [1983]) eliminated that possibility [*Grant et al.*, 1992]. These higher latitude waves exhibited equatorward phase propagation like the SABRE observations, but at latitudes significantly higher than the expected plasmapause position. Analysis of their azimuthal structure revealed azimuthal wavenumbers with magnitudes in the range 45–60, suggesting a similar generation mechanism to the STARE storm-time Pc5 events. Invoking a similar drift resonance generation mechanism then suggested that somewhat lower energy protons (~20 keV) were involved than those driving the STARE observations, with the BARS observations being at higher latitudes. Further analysis of the SABRE results [*Yeoman et al.*, 1992] provided a detailed analysis of the meridional and longitudinal phase propagation of the events. Figure 1.3 presents an example of the spatial structure of the east–west and north–south horizontal velocity components of a wave event observed by the combined fields-of-view of the two overlapping SABRE radars. The Fourier phase of the peak Fourier component (a frequency of 1.7 mHz) for a wave event observed between 1530 and 1600 UT on day 48, 1985 is presented on a 26 × 26 geographic grid. The spatial variation of the Fourier phase reveals a westwards phase propagation in

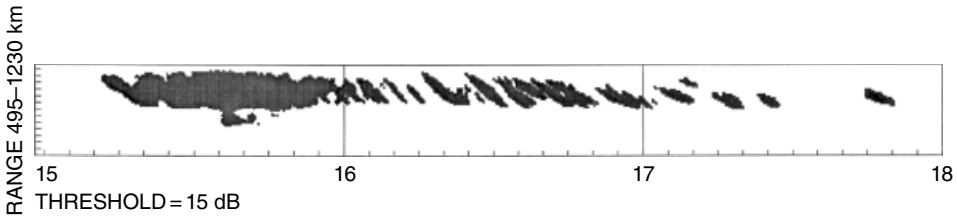

Figure 1.2 Equatorward-moving bands observed in a SABRE range–time–intensity plot. From *Tian et al*. [1991].

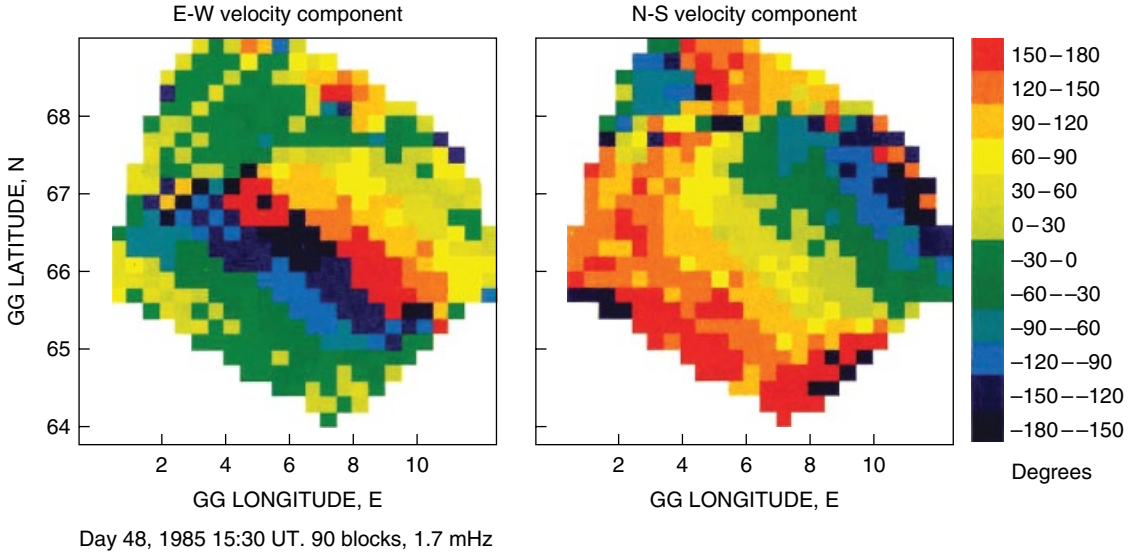

Figure 1.3 Spatial variation of the peak Fourier component at 1.7 mHz frequency of the SABRE East–West and North–South horizontal velocity component for day 48, 1985; 30 minutes of data are processed starting at 1530 UT. From *Yeoman et al*. [1992].

geographic latitude in both the north–south and east–west velocity components, corresponding to an effective azimuthal wavenumber, m, of magnitude between 30 and 40. An equatorward propagation is seen in latitude, and this phase change often exceeded 180°. Such signatures in the radar data were demonstrated to often have no significant corresponding signature in ground magnetometer data. *Yeoman et al*. [1992] suggested that the same drift resonance mechanism proposed by *Grant et al*. [1992] could also be a source for these lower latitude equatorward propagating Pc5 observations, but with particles of similar energies to the earlier STARE storm-time Pc5 results being invoked.

1.3. SUPERDARN OBSERVATIONS

More recent ionospheric observations of high-m ULF waves have taken advantage of the Super Dual Auroral Radar Network (SuperDARN). SuperDARN is a global array of high-frequency (HF) radars. The use of HF frequencies allows radio propagation beyond the horizon, greatly extending the capabilities of the systems compared to the VHF radar systems used in the studies described in Section 1.2. Full details of SuperDARN are given in *Greenwald et al*. [1995] and *Chisham et al*. [2007]. Whilst the radars' design is focused on measuring the global ionospheric convection pattern at a 1 or 2 min cadence, lower frequency ULF waves may be investigated with the standard data products, and a variety of novel scan modes and operations have been devised to allow the study of higher frequency wave regimes. For example, the addition of a second receive channel to some SuperDARN radars allows for so-called stereo operations [*Lester et al*., 2004], where a single or a small number of beams can be sampled on channel B of the radar receivers independently of the main 16 beam scan sampled simultaneously in channel A, in order to improve the temporal resolution of the radars.

The first results on the observation of high-m ULF waves with SuperDARN were performed by *Fenrich et al*. [1995]. They noted many common characteristics between low and high-m waves, including the wave frequencies and their local time occurrence statistics. High-m waves were noted to generally have an equatorward phase propagation, in contrast to the poleward-propagating low-m

events, but their similarities to the low-m waves led to the conclusion that wave–particle interactions could not provide the sole explanation for their occurrence characteristics, although they were likely to be involved in the amplification of the observed wave signatures. These ideas were developed by *Fenrich and Samson* [1997], where a possible explanation for the equatorward phase propagation was included. It was suggested that the latitudinal phase could be reversed in cases where the wave growth via wave–particle interactions exceeded the wave dissipation through the ionosphere, such that the overall Poynting flux was directed outward from the resonance location rather than inward, toward the resonance location.

Following these early SuperDARN studies, the use of active radar techniques, where high-power radiowave transmissions are used to generate backscatter in the SuperDARN radar fields of view, were extensively used over the next few years for the investigation of high-m ULF waves, and these were summarized in *Yeoman et al*. [2006]. More recent results from SuperDARN have provided a wealth of new information on the wave events observed with equatorward phase propagation, as discussed above and in Section 1.2. *Yeoman et al*. [2008] presented data for a high-m wave with an equatorward phase propagation, a period of 300 s and $m \sim -60$, that was observed at very high latitude ($L \sim 15$) over Svalbard during an interval when the open-closed field line boundary had retreated poleward of the high-latitude location. A drift–resonance source in 15 keV protons was inferred, with the high-latitude location shown to preclude the trapping of protons with population inversions at higher energies but to be able to sustain such populations at these lower energies on occasion.

Yeoman et al. [2010] presented a case study of another event observed by the SuperDARN radars at Hankasalmi, Finland, and Þykkvibær, Iceland. The event was associated with a substorm expansion phase, which was detected with the FUV instrument [*Mende et al*., 2000a, b] on the IMAGE spacecraft. Figure 1.4 shows the fields-of-view and data coverage from the SuperDARN radar channel A data, along with three images from the FUV instrument, all in magnetic latitude–magnetic local time coordinates during substorm onset at 2337 UT on 21 March 2002. For this event, the substorm onset occurred within the radar fields of view, with the auroral signature then expanding poleward and westward over the radars. ULF wave observations during the interval are sampled on channel B. These are presented in Figure 1.5, with the Hankasalmi data from a meridional beam (beam 9) presented in Figure 1.5a and the Þykkvibær data in Figure 1.5b. Figure 1.5a clearly shows the equatorward phase propagation of the observed wave. Figure 1.5b shows little phase evolution in the poleward- and westward-oriented beam 5 data from Þykkvibær. Analysis of the wave characteristics showed that this resulted from the combination of the equatorward propagation seen in Figure 1.5a ($\sim 62^{\circ}$ per degree of latitude), and an eastward longitudinal phase propagation corresponding to an azimuthal wave number of $m \sim 13$. *Yeoman et al*. [2010] interpreted these data as implying a wave source in drifting 33 keV particles, with the eastward propagation implying that electrons were the source, rather than protons. Free energy should be available on occasion in the electron populations when the conditions in Equations (1.1) and (1.3) are met for electrons, although in the case of electrons the much more rapid electron bounce period would preclude solutions for conditions other than $N = 0$ in Equation (1.2). The equatorward propagation of the observed wave was explained in terms of a development of the Alfvén ship wave theory elaborated by *Mager and Klimushkin* [2008] and *Mager et al*. [2009].

The case study reported above suggested that both westward-drifting protons and eastward-drifting electrons could drive high-m waves. The relatively modest m value of 13 was suggested to be a result of the close proximity of the wave observations to the substorm onset, where higher energy particles might be available for wave growth. Both these predictions were subsequently tested in a statistical study of similar wave types undertaken by *James et al*. [2013]. In this study 83 similar wave events that were associated with substorm expansion phase onsets identified from IMAGE were analyzed, and their frequencies, latitudinal and longitudinal phase evolution, and proximity to the location of the substorm determined. Figure 1.6 summarizes the findings of the paper. The x-axis of Figure 1.6 shows the longitudinal separation of the substorm onsets and the wave observations. The y-axis illustrates the driving particle energies derived from the wave characteristics, assuming a simple expression for particle drift [*Yeoman and Wright*, 2001] and using Equation (1.3). Westward-drifting particles are inferred for waves west of the substorm onset, and eastward-drifting particles for waves east of the substorm. In both cases, the energy of the particles decreases as the longitudinal separation increases, with the reduced longitudinal drift speed of the lower energy particles implying an increased azimuthal wave number in Equation (1.3). This situation is illustrated schematically in Figure 1.7. Earlier spacecraft observations of similar high- m wave events presented by *Takahashi et al*. [1990] also saw westward azimuthal phase propagation in the dusk sector and eastward phase propagation in the dawn sector, although the waves were not directly correlated with substorm onset locations. In this case the eastward propagation was interpreted as being the result of the Doppler shift imposed by the eastward $\mathbf{E} \wedge \mathbf{B}$ drift in the dawn sector, with westward phase propagation being the case in both sectors in the plasma rest frame. In the case of *Takahashi et al*. [1990] considerably larger phase shifts and higher

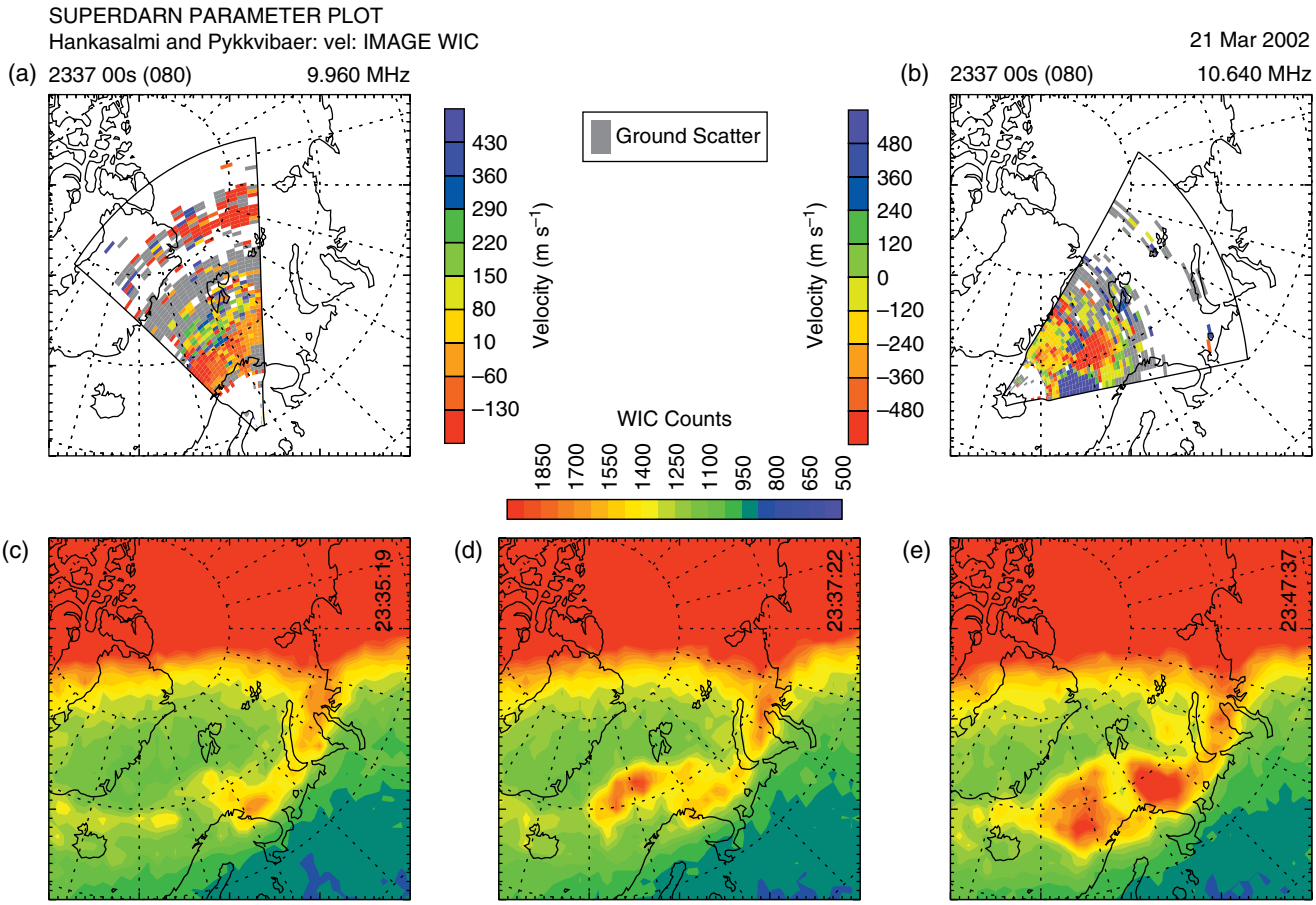

Figure 1.4 Fields-of-view and data coverage from channel A of the SuperDARN radars at (a) Hankasalmi, Finland, and (b) Þykkvibær, Iceland in magnetic latitude–magnetic local time coordinates during substorm onset at 2337 UT. Red (negative) velocities are away from the radar and blue (positive) velocities are toward the radar. The radial dashed lines are separated by 1 hr local time, with local midnight being marked by the vertical dashed line. The dashed circles indicate magnetic latitude at 10° separations. (c–e) present IMAGE WIC auroral data in the same coordinate system for three times during the substorm expansion phase. From *Yeoman et al*. [2010].

wave frequencies were seen in the westward-propagating (dusk) events (where the $\mathbf{E} \wedge \mathbf{B}$ drift added to the proposed wave phase evolution) than in the eastward propagating (dawn) events (where the $\mathbf{E} \wedge \mathbf{B}$ drift subtracted from the proposed wave phase evolution). The events in *James et al*. [2013] were very symmetric in both frequency and phase propagation speed to the east and west of the substorm, and are interpreted as a genuine eastward and westward wave propagation in the plasma rest frame.

1.4. DOPPLER SOUNDER OBSERVATIONS

Opportunities for the study of high-m ULF waves in the ionosphere are not restricted to ionospheric radar systems. HF Doppler sounders offer one such alternative technique. In a Doppler sounder, use is made of the direct reflection of a radio wave from the ionosphere, rather than a scattering process. While a multipoint investigation of the spatial structure of the ULF wave is more difficult with such a system, it does have the advantage of excellent spatial resolution of ~3 – 4km for an F region reflection. Such systems are also simple and inexpensive, and thus can offer continuous operations in a mode suitable for ULF wave investigations, enabling statistical studies to be built up. *Baddeley et al*. [2005a] studied a population of 27 high-m ULF waves from a the DOppler Pulsation Experiment (DOPE), a Doppler sounder located at Tromsø, Norway, at an invariant latitude approximately corresponding to geostationary orbit (an L-shell of 6.3). Direct measurement of the m -number of the waves from two azimuthally separated HF Doppler propagation paths revealed waves with m typically being −100 to −200, representing some of the smallest scale waves ever observed in the ionosphere. Figure 1.8 presents an example of such a wave event, which is clearly visible as a Doppler shift of peak-to-peak amplitude ~1Hz